JOURNAL OF SPACECRAFT AND ROCKETS
Vol. 30, No. 2, March-April 1993

# Electrodynamic Interactions Between a Space Station and the Ionospheric Plasma Environment

J. Wang,* D. E. Hastings,† and M. Martinez-Sanchez†
*Massachusetts Institute of Technology, Cambridge, Massachusetts 02139*

**A general analysis of the electrodynamic interactions between a space station with two exposed charged platforms and the ionospheric plasma is presented. We show that this problem can be separated into a far-field problem, concerned with the electromagnetic interference surrounding the entire space station, and a near-field problem, concentrated on the interactions in the vicinity of the biased platforms. Computer particle simulations as well as approximate analysis were carried out in the near field of the charged platform. Results of the plasma flowfield, the presheath and sheath structure, and current collection characteristics are obtained. The near-field solution is used to construct the perturbation current source in the far-field problem, which is solved by application of plasma fluid theory. It is found that the space station will generate a radiation field composed of the Alfvén waves forming a "wing" structure. Based on our analysis, a global description of the space station's electrodynamic environment is obtained.**

## Nomenclature

| | |
|---|---|
| $\boldsymbol{B}$ | = magnetic field |
| $\boldsymbol{B}_0$ | = geomagnetic field |
| $c, C_A, C_s$ | = speed of light, Alfvén speed, and ion sound speed |
| $d_{sh}$ | = sheath thickness |
| $\boldsymbol{E}$ | = electric field |
| $\boldsymbol{E}^A$ | = Alfvén wave electric field |
| $e$ | = electron charge |
| $I$ | = current |
| $J, j$ | = current density |
| $K$ | = Boltzmann constant |
| $\boldsymbol{k}$ | = wave vector |
| $M$ | = ion flow Mach number |
| $m_e, m_i$ | = electron and ion mass |
| $n_0, n_i, n_e$ | = ambient plasma, ion and electron density |
| $n_0^s, n_i^s$ | = plasma and ion density at the sheath boundary |
| $P_{sh}, P_{\text{presh}}$ | = sheath and presheath power |
| $P_{\text{near}}, P_{\text{rad}}$ | = near-field and far-field power |
| $R_{ce}, R_{ci}$ | = electron and ion Lamor radius |
| $R^{\text{near}}, R^{\text{far}}$ | = near-field zone and far-field zone dimension |
| $T_e$ | = electron temperature |
| $\boldsymbol{u}$ | = velocity |
| $V_0, v_{ti}, v_{te}$ | = orbital, ion thermal and electron thermal velocity |
| $x_1, x_2, x_3$ | = coordinates in the rest frame of the plasma |
| $x_1', x_2', x_3'$ | = moving coordinates with origin at the center box of station |
| $x', y'$ | = moving coordinates with origin at the center of the station projected on the plane $S_A$ |
| $x, z$ | = moving coordinates for a $(x_1', x_3')$ plane cutting through the platform |
| $Z_I, Z_{II}$ | = radiation impedance in band I and band II |
| $Z_{\text{rad}}$ | = total radiation impedance |
| $\alpha$ | = angle of attack |
| $\Gamma$ | = ion flux |
| $\lambda_d$ | = Debye length |
| $\lambda_{\text{mfp}}$ | = mean free path |
| $\lambda_{\text{wave}}$ | = wavelength |
| $\lambda_x, \lambda_\parallel$ | = wavelength component in $x$ and $z$ direction |
| $\Phi$ | = electric potential |
| $\Phi_w, \Phi_{sh}$ | = potential at the plate surface and at the sheath boundary |
| $\theta_0, \theta_A$ | = Mach angle and Alfén angle |
| $\omega_{pe}, \omega_{pi}$ | = electron and ion plasma frequency |
| $\omega_{lh}, \omega_{UH}$ | = lower and upper hybrid frequency |
| $\Omega_e, \Omega_i$ | = electron and ion gyrofrequency |

Presented as Paper 91-0114 at the AIAA 29th Aerospace Sciences Meeting, Reno, NV, Jan. 7-10, 1991; received March 25, 1991; revision received April 30, 1992; accepted for publication May 11, 1992. 

*Currently Member Technical Staff at Jet Propulsion Laboratory, California Institute of Technology, Pasadena, CA 91109.

†Associate Professor of Aeronautics and Astronautics. Member AIAA.

## I. Introduction

A CHARGED object in space will interact with the plasma environment through electromagnetic forces. The presence of a space station in the ionosphere will cause a very complex set of electrodynamic interactions. The space station is attached to many charged parts such as solar arrays and certain onboard experimental devices, which will interact with the ambient plasma. Exposed voltages will drive a current flow into and out of the space station through any uninsulated surfaces. Therefore the entire space station is also a moving current source, which could excite plasma wave radiation in the ionosphere. The effects of the electrodynamic interactions between a space station and the plasma environment appear in many ways. The local interactions in the vicinity of the exposed high-voltage parts may lead to many undesirable consequences, such as the erosion of metallic surfaces by the impact of energetic ions, power drain due to leakage currents, degradation of solar cell material due to arc discharges, etc. The induced wave radiation in a space station's global environment not only results in a radiation power loss, but it also leads to electromagnetic pollution which may have a negative impact on the operations of some electromagnetically sensitive devices and space plasma measurements.

The physics of a charged body immersed in a quiescent plasma is generally well understood. Studies of such a subject have been developed into an important discipline known as probe theory. This probe theory has been adequate in studying the satellite-plasma interactions at geosynchronous Earth orbit (GEO).[1] However, the nature of the interactions related to a space station at low Earth orbit (LEO) is far more complicated than that related to a GEO satellite. The charged parts

of a space station usually have large dimensions and high voltages (for example, the Space Station Freedom's solar array panel will be about 20 m long, 10 m wide, and 2.5 cm thick, and have a surface voltage $\Delta\Phi \sim 160$ V). The resulting nonlinear interaction with the local high-speed plasma flow is unfortunately in a regime that cannot be treated by existing probe theories. In addition, a moving spacecraft at LEO sees a motion induced emf $\boldsymbol{V}_0 \times \boldsymbol{B}_0$ of about 0.24 V/m. The effect of the $\boldsymbol{V}_0 \times \boldsymbol{B}_0$ electric field increases with the size of the structure. Hence, the interaction at LEO has to be treated as an electrodynamic problem determined by the full set of Maxwell's equations because the effects of induced wave radiation usually cannot be neglected.

There have been many recent studies of interactions related to LEO space systems, such as plasma sheath and wake,[2-5] induced wave radiation,[6-9] interactions of high-voltage solar array,[10-12] etc. Since most of these studies concentrated only on specific aspects of the problem, they cannot be applied to provide a global picture of interactions induced by a space station. The NASCAP/LEO and POLAR codes have also been successful in modeling many spacecraft interaction problems.[13-17] However, the codes' formulation limits their applications mainly to electrostatic interactions.

Tne purpose of this paper is to develop a general analysis of the basic electrodynamic interactions between a space station and the ionospheric plasma. The problem is analyzed in Sec. II. The essential elements of the electrodynamic interactions include local-scale interactions in the vicinity of the space station's charged parts as well as global-scale interactions surrounding the entire space station. (There are also many microscale interactions which may have a significant impact on the space station; e.g., the arcing problem at the interconnectors between the solar cells, critical ionization velocity phenomena in certain artificial plasma environments, etc. These microscale phenomena will not be considered in this paper.) In this paper, the local-scale interactions are solved under a near-field formulation. This near-field solution is used to construct a perturbation current source to represent the space station. We then solve the global-scale interactions in a far-field problem. The near-field interactions of a positively biased object in LEO can be studied by using the theory of a stationary probe in a strong magnetic field. However, a major portion of the space station's structure will be biased below the plasma potential, sometimes at a very negative voltage. Since nonlinear interactions of a large, negative body with a high-speed plasma flow are generally not well understood, in Sec. III we shall first carry out a general analysis of the near-field plasma flow over a negatively charged plate. The far-field wave radiation by a moving current source in plasma has been a subject of many recent studies. However, most of these studies are performed specifically for the tethered-satellite system. Based on a general theory of radiation by Barnet and Olbert,[6] Wang and Hastings recently analyzed a current source with a space-station-like structure.[18] Based on the analysis developed in Ref. 18 and Sec. III, we proceed in Section IV to study the interactions of a generic space station model. Sec. V contains discussions and conclusions.

## II. Analysis of the Problem

In Fig. 1a, we illustrate a space station model orbiting in the ionosphere. A typical dayside plasma environment at 300 km is a mainly $O^+$ plasma with electron and ion number density $n_e = n_i \simeq 2 \times 10^5$ cm$^{-3}$. The Earth's magnetic field is about $B_0 = 0.33$ G. The basic plasma parameters are listed in Table 1.

Since our purpose is to study the basic local-scale and global-scale interactions, we shall consider a simplified space-station model shown in Fig. 1b. The structure is taken to be moving in the $-x_1$ direction at a velocity $V_0 \sim 8$ km/s across the geomagnetic field, which is in the $x_3$ direction. This space-station-like structure has an $80 \times 5 \times 5$-m center box section C (with insulated surfaces) oriented along the $\boldsymbol{V}_0 \times \boldsymbol{B}_0$ direction

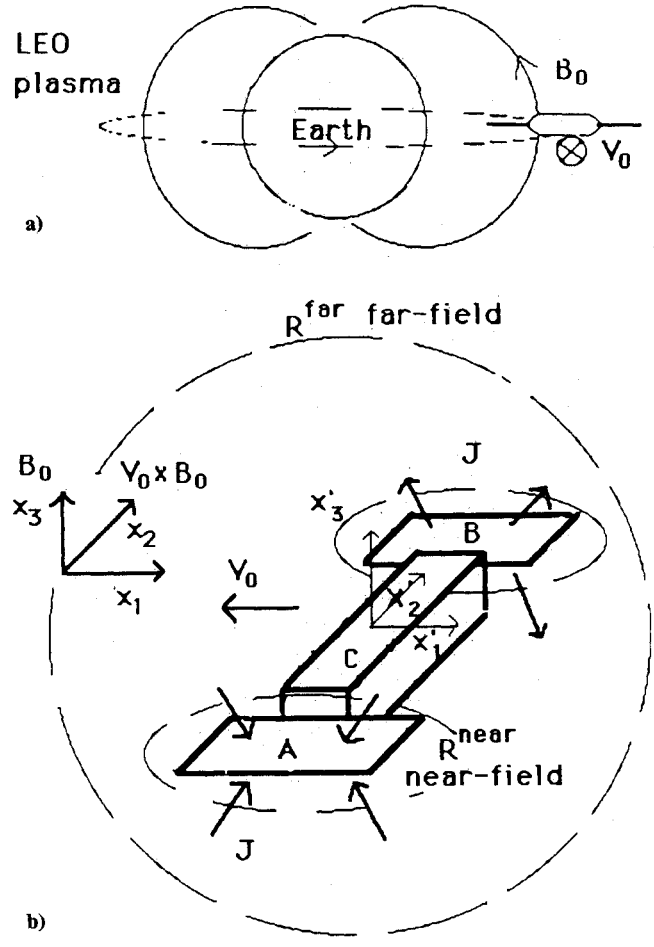


**Fig. 1 Space-station model: a) space station in low Earth orbit; and b) model structure, near-field zone, and far-field zone.**

**Table 1 Basic plasma parameters**

| | |
|---|---|
| Temperature, eV | $T_e \sim T_i \sim 0.1$ |
| Thermal speed, m/s | $v_{te} \sim 1.5 \times 10^5$ |
| | $v_{ti} \sim 8 \times 10^2$ |
| Ion sound speed, m/s | $C_s \sim 1 \times 10^3$ |
| Mean free path of ions and electrons, m | $\lambda_{mfp} \sim 10^2$ |
| Debye length, cm | $\lambda_d \sim 0.6$ |
| Ion/electron gyrofrequency, Hz | $\Omega_i \simeq 31$ |
| | $\Omega_e \simeq 1.6 \times 10^6$ |
| Ion/electron plasmafrequency, Hz | $\omega_{pi} \simeq 2.3 \times 10^4$ |
| | $\omega_{pe} \simeq 4.0 \times 10^6$ |
| Lower/upper | $\omega_{lh} \simeq 5.3 \times 10^3$ |
| hybrid frequency, Hz | $\omega_{UH} \simeq 4.1 \times 10^6$ |

and two thin conducting platforms A and B with area $20 \times 10$ m each. Platforms A and B could be solar array-wings with exposed interconnectors or platforms that contain other high-voltage electric systems. The space station is electrically coupled with the ionosphere through platforms A and B, which are connected through some internal circuit inside section C. In a steady state, the potential distribution over the structure is such that it collects no net current from the plasma. To simulate the currently designed negative grounding configuration, we assume our space-station model is grounded at platform B while platform A is overall charged to a negative potential with respect to the plasma. Such a potential distribution is a very simplified model. To determine the potential distribution over a real space station (which can be quite complicated), one needs to analyze the detailed locations of all of the electrical systems onboard. Such a task is beyond the scope of this paper. We assume there is no active electron beam emission involved. The total current is determined by

the ion current collection at platform A, which is balanced by the electron current collection at platform B. Therefore, the current flows into the structure through A and out through B.

Most generally the electrodynamic interactions between the space-station model and the plasma are determined from the plasma kinetic equations, Maxwell's equations

$$\nabla \cdot \boldsymbol{E} = 4\pi\rho_c$$

$$\nabla \cdot \boldsymbol{B} = 0$$

$$\nabla \times \boldsymbol{E} = \frac{1/c\,\partial \boldsymbol{B}}{\partial t}$$

$$\nabla \times \boldsymbol{B} = 4\pi/c\boldsymbol{J} + \frac{1/c\,\partial \boldsymbol{E}}{\partial t}$$

and the boundary conditions at the object-plasma interface. Except for a few extremely simple cases, solving such a system is a very difficult endeavor.

We notice that the interactions induced by the space station have different characteristics in different regions of the environment. The local environment in the vicinity of the conducting platform is dominated by plasma flow-charged body interactions, while the global environment surrounding the entire space station is mainly affected by the induced wave radiation. Therefore our basic approach is to separate the interactions on different scales. We separate the interaction domain into a far-field zone surrounding the entire space station and two near-field zones, which are in the vicinity of the charged platforms. The far-field zone ($r \geq R^{\text{far}}$) and near-field zone ($r \geq R^{\text{near}}$) are illustrated in Fig. 1b.

Let us first consider the interactions in the far field. In the far-field zone of a large structure (dimension $L_{\text{station}}$), we have $r \geq R^{\text{far}} > L_{\text{station}} \sim \lambda_{\text{mfp}}$. Hence, a fluid description is usually sufficient for analysing the far-field phenomena. The governing equations in the far field are Maxwell's equations and the cold plasma fluid equations:

$$\frac{\partial n_j}{\partial t} + \nabla \cdot (n_j \boldsymbol{u}_j) = 0, \qquad j = i,e \tag{1}$$

$$\frac{m_j n_j\, \partial \boldsymbol{u}_j}{\partial t} + \boldsymbol{u}_j \cdot \nabla \boldsymbol{u}_j = q_j n_j (\boldsymbol{E} + \boldsymbol{u}j \times \boldsymbol{B}), \qquad j = i,e \tag{2}$$

The effects of nonlinear interactions caused by a high-voltage platform are mostly limited to its sheath layer where substantial charge separation occurs. Therefore, it is reasonable to assume the perturbation in the far field is small enough that the fluid equations can be linearized. The condition for the linear assumption to be valid can be written as $B'/B_0 \ll 1$, or equivalently

$$E'/V_0 B_0 \ll 1 \tag{3}$$

where $E'$ and $B'$ are the perturbed electromagnetic (EM) field measured in the moving frame and $B_0$ is the geomagnetic field. For $V_0 \simeq 8$ km/s and $B_0 = 0.3$ G, we have the background electric field $E_0 = V_0 B_0 \simeq 0.24$ V/m.

For the far-field plasma, the space station represents a perturbation current source. To obtain the disturbances generated by this current source, we use a Laplace transform in time and Fourier transform in space to solve Maxwell's equations and the plasma fluid equations. The governing equation for the perturbed electric field is a wave equation, which in the $(\boldsymbol{k},\omega)$ space is written as[6]

$$\boldsymbol{k} \times [\boldsymbol{k} \times \boldsymbol{E}(\boldsymbol{k},\omega)] + (\omega^2/c^2)\tilde{K} \cdot \boldsymbol{E}(\boldsymbol{k},\omega)$$

$$= -4\pi(i\omega/c^2)\boldsymbol{J}_s(\boldsymbol{k},\omega) \tag{4}$$

where $\tilde{K}$ is the dielectric tensor and $\boldsymbol{J}_s(\boldsymbol{k},\omega)$ is the current source function.

The ionospheric plasma response to an external current source has been studied in detail by many authors recently. A general analysis for cold plasmas was presented by Barnett and Olbert. A formal solution of the electromagnetic field can be written as[6]

$$\boldsymbol{E}(\boldsymbol{k},\omega) = -4\pi i\omega/c^2 \tilde{T}^{-1} \cdot \boldsymbol{J}_s(\boldsymbol{k},\omega)$$

$$\boldsymbol{\beta}(\boldsymbol{k},\omega) = c/\omega \boldsymbol{k} \times \boldsymbol{E}(\boldsymbol{k},\omega) \tag{5}$$

where the tensor $\tilde{T}$ is defined by $\tilde{T} = -k^2\tilde{I} + \boldsymbol{kk} + \tilde{K}\omega^2/c^2$. Analyzing the dispersion relation, it is found that a moving current source in the ionosphere will induce Alfvén waves and lower hybrid waves. In the rest frame of the plasma the Alfvén waves have a frequency band from zero to the ion gyrofrequency ($\Omega_i \simeq 30$ Hz) and the lower hybrid waves from the lower hybrid frequency ($\omega_{lh} \simeq 5$ kHz) to the electron gyrofrequency ($\Omega_e \simeq 0.9$ MHz). The electromagnetic field in ordinary space can be obtained by calculating the inverse Laplace-Fourier transform on Eq. (5). Readers are referred to Refs. 6 and 18 for details of such calculations.

The far-field wave structure is found to be some function of the divergence of the source current and the wave magnitude is proportional to the total strength of the source current. Therefore the far field can be solved only if we know the current source $\boldsymbol{J}_s$. A self-consistent treatment of the current source proves to be extremely difficult within the fluid formulation discussed previously. A common practice in all of the previous studies of the induced-radiation problem is to assume some ad hoc model for the current source. Such a practice is feasible only when the current collecting system is simple enough so that one can make a reasonable guess of the strength and distribution of the source current.

We next consider the interactions in the vicinity of the charged plates. The purpose of the near-field problem is not only to determine the current source for the far-field problem, but also to analyze the local environment of the charged plates. In the near-field region, the above far-field formulation breaks down because cold plasma fluid equations are not a very good approximation to the near-field rarefied plasma. In addition, when the platforms are biased to a very high voltage, local disturbances are almost certainly nonlinear. Although the linear fluid approximations are no longer valid, an electrostatic approximation may be made to simplify the near-field problem. Let us denote $\lambda_{\text{wave}}$, to be the characteristic wavelength of the far-field EM waves generated by the space station ($\lambda_{\text{wave}}$ will be determined in Sec. IV). If the near-field zone is well within one wavelength, i.e.,

$$R^{\text{near}} \ll \lambda_{\text{wave}} \tag{6}$$

then the electric field in the near field can be approximately determined from Poisson's equation.

[The condition stated in Eq. (6) can be explained as follows: We consider the plasma as a medium with permittivity $\epsilon$ and permeability $\mu$. The electric field can be expressed by the scalar and vector potentials, $\Phi$ and $\boldsymbol{A}$,

$$\boldsymbol{E} = -\nabla\Phi - \frac{1}{c}\frac{\partial \boldsymbol{A}}{\partial t}$$

where $\Phi$ and $\boldsymbol{A}$ satisfy

$$\nabla^2\Phi + \frac{\epsilon\mu}{c}\frac{\partial^2\Phi}{\partial t^2} = -\frac{4\pi}{\epsilon}\rho_c \tag{7a}$$

$$\nabla^2 \boldsymbol{A} - \frac{\epsilon\mu}{c}\frac{\partial^2 \boldsymbol{A}}{\partial t^2} = -\frac{4\pi\mu}{c}\boldsymbol{J} \tag{7b}$$

Equation (7) scales as

$$\frac{\Phi}{r^2} + \frac{1}{V_{\text{wave}}^2}\frac{\Phi}{2} \sim \frac{4\pi}{\epsilon}\rho_c$$

where $V_{wave} = c/\sqrt{\epsilon\mu}$ is the characteristic wave speed in the medium. Within the region $r \ll \lambda_{wave}$, the wave propagation speed can be regarded as infinite. Therefore, if the dimension of the near-field zone satisfies $R^{near} \ll \lambda_{wave}$, we have

$$\nabla^2\Phi + \frac{\epsilon\mu}{c}\frac{\partial^2\Phi}{\partial t^2} \simeq \nabla^2\Phi \simeq \frac{4\pi}{\epsilon}\rho_c, \qquad \text{or} \qquad E \simeq \nabla\Phi$$

within $r \leq R^{near}$. Based on this discussion, a good definition for the far-field zone and near-field zone is $R^{near} < \lambda_{wave} < R^{far}$.]

We have separated the problem into a far-field problem concerned with the electromagnetic interference surrounding the entire space station, and a near-field problem, concentrated on the interactions in the vicinity of the charged platforms. One usually needs to iterate between the far field and the near field in order to construct a solution for the entire region. However, as we shall show in Sec. IV, for our space station model the interaction in the near field is much stronger than that in the far field. Therefore, we may neglect the effects of far-field radiation in the near-field problem. Let us define $P_{rad}$ to be the power carried by the far-field waves and $P_{near}$ the power drain within the near-field region. The level of the far-field and near-field interaction can be compared through $P_{rad}$ and $P_{near}$. Hence, if we have

$$P_{rad} \ll P_{near} \tag{8}$$

then the far-field and near-field problem can be decoupled.

## III. Near-Field Plasma Flow over a Charged Plate

In this section, we study the near-field plasma flow charged object interactions. The important, large-dimensional charged parts of a space station, such as the solar arrays, are in the shape of thin platforms. Usually almost the entire portion of such a platform is biased below the plasma potential. Therefore the interaction of a negatively biased thin platform is of particular interest.

We consider a two-dimensional plate and solve the problem in the moving frame fixed with the plate (Fig. 2). In the moving frame, there is a background field $E_0 = V_0 \times B_0/c$. We define the electric potential in the moving frame as

$$\Phi_{moving} = \Phi_{rest} - \frac{x_2'}{c} V_0 \times B_0$$

where $x_2'$ is an arbitrary distance along the $V_0 \times B_0$ direction. We can set $x_2' = 0$ for our two-dimensional problem. We shall make the following simplifications:

1) Since $v_{te} \gg V_0$, the electron number density in the vicinity of a negatively biased platform is given by

$$n_e = n_0 \exp\frac{e\Phi(r)}{KT_e}$$

2) Since $v_{ti} \ll V_0$, we can neglect the effects of the thermal motion of the ions. Furthermore, the geomagnetic field effect on the ion motion can be neglected because the Larmor radius of the ions $R_{ci} = V_0/\Omega_i \simeq 36$ m is usually large compared to the dimension of the plate. Therefore an observer on the plate sees a uniform oncoming ion flow with velocity $V_0$. We can define the Mach number using the ion sound speed $C_s = \sqrt{KT_e/m_i}$. The ambient oncoming ion flow has a Mach number $M_0 = V_0/C_s \simeq 8$.

3) The plate surface is taken to be a perfect absorber biased at a certain potential $\Phi_w$. The ions are assumed to be neutralized after they hit the surface.

4) We assume that Eq. (6) and Eq. (8) are satisfied.

With these assumptions, the electric field in the near field is governed by

$$\nabla^2\Phi = -4\pi e\left[n_i - n_0 \exp\frac{e\Phi}{KT_e}\right] \tag{9}$$

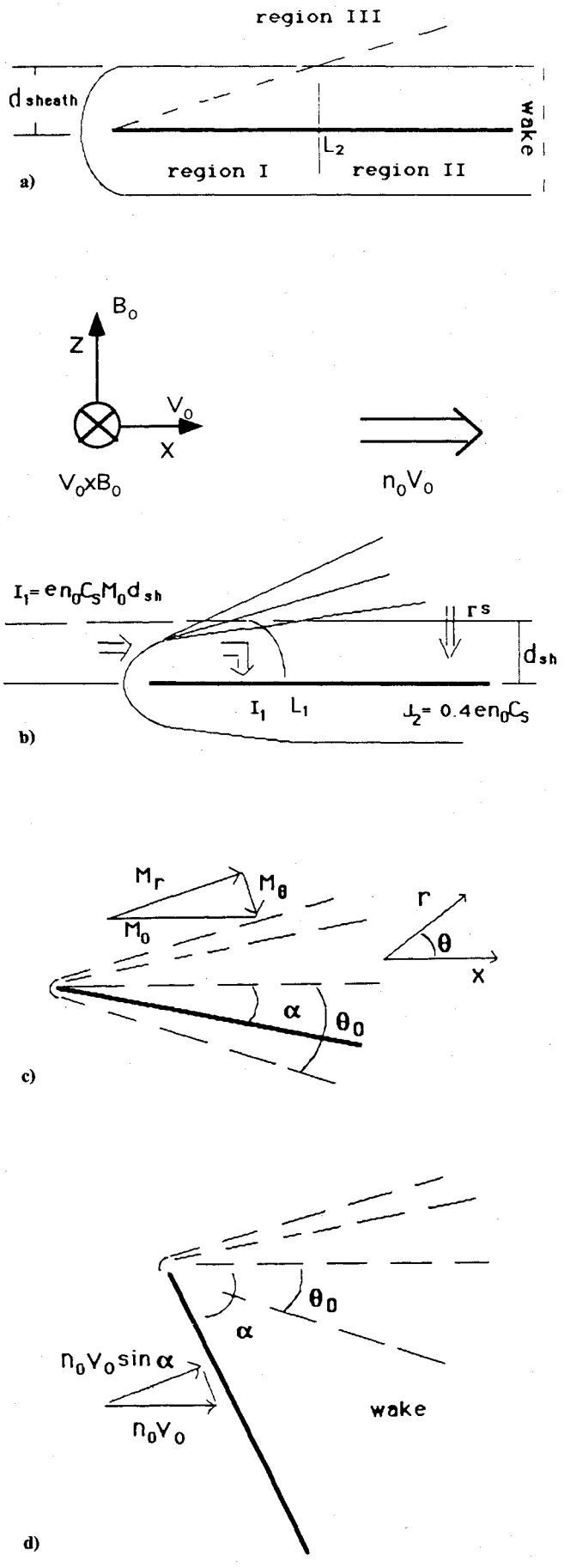


**Fig. 2 The near-field plasma flow: a) zero angle-of-attack situation; b) current collection at zero angle of attack; c) small angle-of-attack situation ($\alpha < \theta_0$); and d) large angle-of-attack situation ($\alpha < \theta_0$).**

where $\Phi = -\Phi_w$ at the platform surface and $\Phi = 0$ at infinity. The ion density $n_i$ is obtained from the positions of the ion particles. The motion of each individual ion particle is determined by

$$m_i \frac{du}{dt} = -e\nabla\Phi \tag{10}$$

We have developed a two-dimensional hybrid particle simulation code to solve the near-field problem. In the code the plasma is composed of particle ions and fluid electrons. The ion flowfield, the space charge, and the nonlinear Poisson's equation are solved self-consistently by tracking the motion of representative ion particles. The code resolves the physics on the ion-plasma time scale.

We first study a plate with a uniform potential distribution at a zero angle of attack. To understand the physics underlying the plate-plasma interactions, we begin by analyzing the plasma flowfield. The plasma flowfield can be divided into a quasineutral region (region III), a wake, and a sheath of significant charge separation adjacent to the plate surface. We further divide the sheath layer into a region I (which includes the leading edge) and a region II (which is the fully developed sheath layer) (see Fig. 2a).

An analytical treatment can be carried out for the situation of a very long plate with a very thin sheath (i.e., when the leading-edge effect can be neglected). In region III, from the quasineutral assumption $n_i \simeq n_e$, we have

$$e\nabla\Phi \simeq KT_e \frac{\nabla n_i}{n_i}$$

The Poisson's equation and the ion continuity and momentum equation in region III can be combined to give:

$$\nabla \cdot (n_i m_i u) = 0 \tag{11}$$

$$n_i m_i (u \cdot \nabla)u + \nabla(n_i KT_e) \simeq 0 \tag{12}$$

We observe that these two equations are exactly the continuity and momentum equations of a compressible gas flow with the pressure $P = n_i KT_e$. Therefore, in region III, our problem is similar to a supersonic gas flow problem. However, the gas flow is isothermal under our assumptions.

In region II (the region far behind the leading edge), the potential varies rapidly only in the $z$ direction for the fully developed sheath layer. Hence, we have $\partial/\partial z \gg \partial/\partial x$. Therefore the ion motion in region II is approximately given by:

$$\Gamma = n_i u_z \simeq \text{const}, \qquad u_x \simeq \text{const}$$

$$u_z \frac{\partial u_z}{\partial z} \simeq -\frac{e}{m_i}\frac{\partial \Phi}{\partial z}$$

Hence in region II one need only to consider the ion motion in the $z$ direction.

The solutions to regions II and III are connected by the boundary condition at the region II/ III interface. This condition is that there is a vertical particle flux $\Gamma^s = n_i^s u_z^s$, where $n_i^s$ and $u_z^s$ are the ion density and velocity at the sheath edge.

If the sheath is infinitely thin compared to the scale of region III, the boundary condition of vertical ion flux $\Gamma = \Gamma^s$ yields the solution in region III to be an expansion fan centered at the leading edge, which is similar to the Prandtl-Meyer expansion of a supersonic gas flow over a convex corner. The outer envelope of the expansion fan is at an angle of $\theta_0 = \sin^{-1}(1/M_0) \simeq 1/M_0$. This expansion fan is a presheath. The presheath disturbances are ion sound waves. As an ion goes through the presheath region, its trajectory will be turned toward the plate in such a way that the component of its velocity normal to the expansion characteristic lines is always sonic. The turning of the ion trajectory is given by

$$d\theta_i = \sqrt{M^2 - 1}\,\frac{dM}{M}$$

Now we consider the sheath layer. The electric field in region II is similar to that in a one-dimensional planar sheath:

$$\frac{\partial^2\Phi}{\partial z^2} \simeq -4\pi e\left[\frac{n_i^s}{\sqrt{1 - 2(\Phi - \Phi_{sh})/m_i u_z^{s2}}} - n_0 \exp\left(\frac{e\Phi}{KT_e}\right)\right] \tag{13}$$

For a physical solution to exist, the ions must satisfy the Bohm sheath criterion as they enter region II (i.e., the sheath):

$$u_z^s \geq C_s$$

When $-\hat{\Phi}_w = -e\Phi_w/KT_e \gg 1$, the sheath thickness in region II is given by the well-known Child-Langmuir law:

$$\left(\frac{d_{sh}}{\lambda_d^s}\right)^2 = \frac{4\sqrt{2}}{9}\frac{|\hat{\Phi}_w|^{3/2}}{M_s} \tag{14}$$

Where $\lambda_d^s = \sqrt{KT_e/4\pi n_0^s e^2}$ is defined using the plasma density at the sheath edge and $M_s = u_z^s/C_s$.

Connecting the solutions in regions II and III, one finds that the sheath boundary can be defined as the final expansion characteristic, which is parallel to the plate. Hence, the ions enter the sheath with a vertical velocity equal to the ion sound speed, $u_z^s = C_s$. The potential at the sheath boundary is found to be

$$\Phi_{sh} = -\frac{KT_e}{2e}\sin^{-1}\left[\frac{1}{M_0}\left(2\sqrt{M_0^2 - 1} + \sin^{-1}\frac{1}{M_0}\right)\right] \simeq -\frac{KT_e}{e} \qquad \text{for } M_0 \gg 1$$

and the plasma density at the sheath boundary $n_0^s \simeq n_0 \exp(-1)$. The sheath thickness is given by Eq. (14) with $M_s = 1$:

$$d_{sh} \simeq 0.8|\hat{\Phi}_w|^{3/4}\lambda_d^s \simeq 1.3|\hat{\Phi}_w|^{3/4}\lambda_d \tag{15}$$

A similar analysis of regions II and III was first presented by Lam and Greenblatt.[19]

Note the preceding analysis is valid only when the sheath can be regarded as infinitely thin compared to the expansion fan region. The thickness of the expansion fan at a distance $L$ from the leading edge is $D_{presh}(L) \simeq \tan(\theta_0)L \simeq M_0 L$. Let us define a distance $L_2$ such that $D_{presh}(L_2) = d_{sh}$, $L_2$ is given by

$$\frac{L_2}{d_{sh}} = \cot\theta_0 \simeq M_0, \qquad \text{or} \qquad \frac{L_2}{\lambda_d} \simeq 1.3M_0|\hat{\Phi}_w|^{3/4} \tag{16}$$

The expansion characteristic lines extend far outside the sheath only at a distance far behind the leading edge $L \gg L_2$. Therefore the preceding analysis is valid for the region $L \gg L_2$. From the preceding analysis, the vertical ion flux entering the fully developed sheath layer is $\Gamma^s = n_i^s u_z^s \simeq n_0^{\exp-1} C_s$. Therefore, from the ion flow continuity, the ion current collected by the portion of the plate in region II is independent of the surface potential and has a uniform density:

$$J(L > L_2) = J_2 = e\Gamma^s \simeq 0.4en_0 C_s \tag{17}$$

For a thin plate at a zero angle of attack, we note from Eq. (14) that the sheath can be very "thick" for a high-voltage plate. For instance, a solar array has a typical surface potential $\Phi_w = -160$ V. The sheath layer adjacent to the solar-array surface will have a thickness $d_{sh} \sim 328\lambda_d \sim 2$ m. One of the direct consequences of the thick sheath is that the region I sheath will cover a fair portion of the plate, where the given

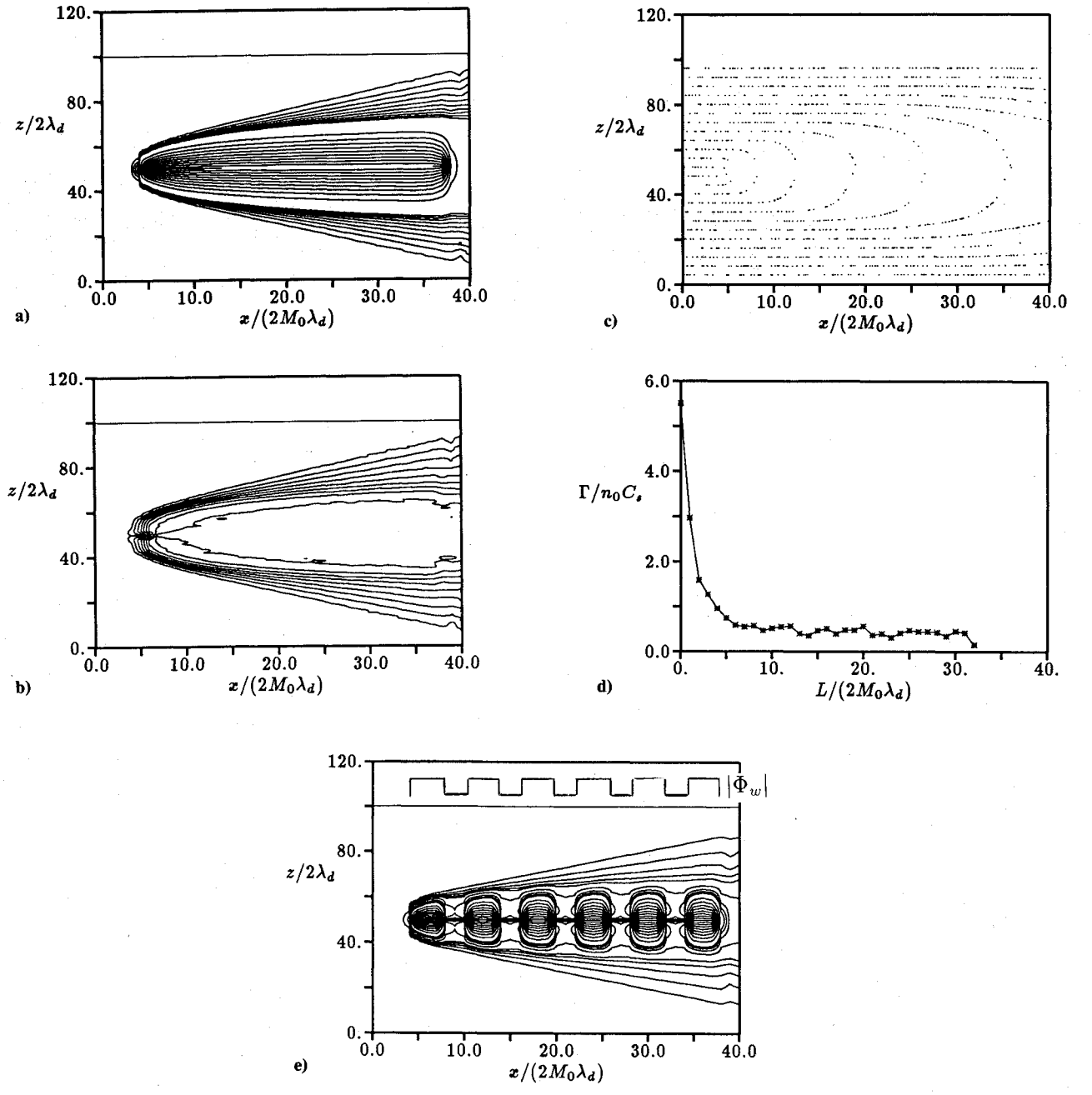


**Fig. 3 Particle simulation results for zero angle of attack ($\hat{\Phi}_w = -80$, $M_0 = 8$, length of the plate $L_{tot}/M_0\lambda_d = 64$). Location of the plate $z/2\lambda_d = 50$, $5 \leq x/(2M_0\lambda_d) \leq 37$: a) potential contours: uniform surface voltage (outer expansion fan region: $|\hat{\Phi}|$ from 0.1 to 1, increment 0.1; inner sheath region: $|\hat{\Phi}|$ from 0.1 $\hat{\Phi}_w$ to $\hat{\Phi}_w$, increment 0.1 $\hat{\Phi}_\omega$); b) ion density contours ($n_i$ from 0.1 to 0.9, increment 0.1); c) ion streamlines; d) distribution of ion collection over the plate; and e) potential contours; periodic surface voltage (outer expansion fan region: $|\hat{\Phi}|$ from 0.2 to 1, increment 0.2, inner sheath region: $|\hat{\Phi}|$ from 0.1 $\hat{\Phi}_w$ to $\hat{\Phi}_w$.**

analytical solution breaks down. For $\Phi_w = -160$ V and $M_0 = 8$, we find $L_2 \simeq 16$ m. The plasma flow in region I is too complex for one to study it analytically. Therefore, to find the plasma flowfield and the sheath surrounding a high-voltage plate, a numerical solution is unavoidable.

In Fig. 3, we present a typical set of particle simulation results for a zero angle of attack plate. In Fig. 3a, we plot the potential contours. Figure 3b shows the ion number density contours. Figure 3c shows the steady-state ion streamlines. The potential contours in Fig. 3a clearly show an expansion fan formed from the leading edge. Far behind the leading edge, the potential contours coincide with the straight line expansion characteristics obtained analytically. Near the leading edge, these contours become curved due to the leading-edge effects. The asymptote of the outer envelope has an angle $\theta_0 \simeq 1/M_0 = 0.125$. The expansion fan is the presheath. The potential contours in the presheath gradually turn parallel to the plate. Near the plate surface the ions enter the sheath region where the potential contours are at values $-\Phi > \mathcal{O}(KT_e/e)$.

In Fig. 3d, we show the ion collection distribution over the plate length $L$ obtained from particle simulations. The result shows that there is a great concentration of ion collection at the tip of the leading edge. This concentration is due to those ions captured by the front side of the sheath layer. We may define a leading-edge distance $L_1$ by

$$\int_0^{L_1} J\,dL = I_1 = en_0C_sM_0d_{sh} \tag{18}$$

where $I_1$ is the ambient current flux within a cross section of $d_{sh}$ (see Fig. 2b). We find $L_1 \sim L_2$. The strength of the current density falls very quickly within the leading-edge region. The result shows that the current collection by the plate at $L > L_2 \sim L_1$ is uniform and independent of the surface potential with a density $J_2 \simeq 0.4en_0C_s$. It is interesting to note that although the current density over the major portion of the plate surface is of the order of $en_0C_s$, the current collection near the leading edge may dominate the total current collection for a high-voltage plate because of its dependency on the surface potential.

In Figs. 3a–3d, we assumed the plate is biased at a uniform surface potential. In a real situation, the potential on a solar-array wing surface often has a periodic distribution. In their study of high-voltage solar arrays, Kuninaka and Kuriki[10] modeled the solar array as a single conducting plate based on the assumption that it is covered by a single sheath. To verify their assumption, we performed particle simulations for a plate with a periodic surface potential. The potential contours are plotted in Fig. 3e. The result shows that the sheath of the conducting connectors will overlap each other if the surface potential $|\Phi_w|$ is high enough. As a result, a uniform sheath layer is formed covering the entire plate. Hence the overall effect on the ion motion is very similar to that of a conducting plate with a uniform potential. Therefore, if one is interested only in interactions on the scale of the entire plate, the plate can usually be treated as if it were biased at a uniform potential. Results for a plate with nonuniform potential distributions can be found in Ref. 20.

A plate at a zero angle of attack has the minimum drag. However, in a practical situation the space station's conducting platform can have a wide range of angles of attack. For a plate at a nonzero angle of attack, the quasineutral solution can be obtained by solving Eqs. (11) and (12) in polar coordinates. When the plate is at a small angle of attack $\alpha < \theta_0 \simeq 1/M_0$ ($\theta_0 = 7.1$ deg for $M_0 = 8$), there is an expansion fan presheath on both sides (Fig. 2c). The expansion characteristics are given by

$$M_\theta = \pm 1, \qquad M_r = \sqrt{M_0^2 - 1} + |\theta_0 - \theta|$$

Therefore the problem is very similar to the zero angle-of-attack problem. When the plate is at a large angle of attack $\alpha > \theta_0$, the ions are hitting the front side of the plate at a normal velocity $v_n = V_0 \sin\alpha > C_s$ (Fig. 2d). Except for a very thin sheath layer [the thickness is given by Eq. (14) with $M_s = M_0 \sin\alpha$], the plasma flowfield in front of the plate is unperturbed. The edge of the plate will only generate one family of characteristics, constituting the expansion fan in the wakeside. We performed particle simulations to study the wake region. Some of the typical simulation results are presented in Fig. 4. The potential contours and ion flux field for $\alpha = 90$ deg are shown in Figs. 4a and 4b and those for $\alpha = 45$ deg are shown in Figs. 4c and 4d. As predicated by the analytical solution, the far wake of the plate is composed of the expansion waves generated by the edge of the plate. The region right behind the plate is vacuum. Hence, the current collection at a large angle of attack is dominated by the ram ion flux connected by the front side of the plate: $I = en_0V_0A \sin\alpha$. It is interesting to note that the finite sheath thickness at the edge of the plate will generate an ion-rich stripe downstream (an embedded sheath), which separates the ion void region and the quasineutral expansion wave region. At a very negative surface potential, the embedded sheath may curve enough to strike the rear of the plate resulting in a localized current density. However, the total backside current is usually much smaller than the frontside current. The mechanism formulation of such a wake structure is discussed in detail in Ref. 21.

## IV. Electrodynamic Interactions of a Space Station

We now apply the results and methods of Sec. III and Ref. 18 to study the electrodynamic interactions induced by our

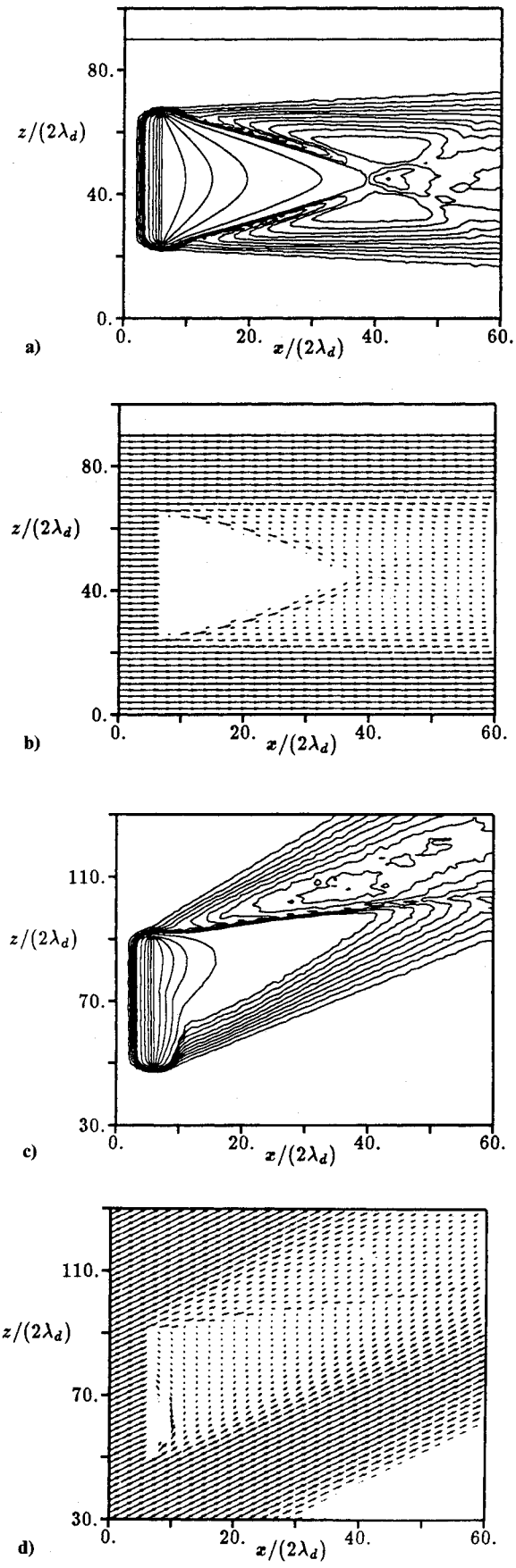


**Fig. 4 Particle simulation results for nonzero angle of attack ($\hat{\Phi}_w = -20$, $M_0 = 8$, length of the plate $L_{tot}/\lambda_d = 80$): a) and b) potential contours and ion flux field for $\alpha = 90$ deg; c) and d) potential contours and ion flux field for $\alpha = 45$ deg. (Potential contour levels in a and c: $|\hat{\Phi}|$ from 0.2 to 2 with increment 0.2 and from $0.2|\hat{\Phi}_w|$ to $|\hat{\Phi}_w|$ with increment $0.2|\hat{\Phi}_w|$).**

space-station model shown in Fig. 1b. The space station's platforms are assumed to be at a zero angle of attack. We shall first study the nearfield of the station's charged platforms. We then construct the current source and calculate the far-field environment of the entire structure.

The physics of a two-dimensional plate interacting with the plasma flow was studied in detail in the last section. Except at the edge of the platform, the analysis of Sec. III can be directly applied to platform A. Figure 5 shows the vector ion flux *nu* and the potential contours within the sheath on a $(x_1', x_3')$ plane cutting through platform A. In Fig. 5a, we take the surface voltage to be $-50$ V. The sheath layer is fully developed at $L > L_2 \sim 7$ m. In Fig. 5b, we take the surface voltage to be $-160$ V. For such a high voltage, almost the entire plate is within region I. The sheath layer appears like a wedge shape. The thickness of the fully developed sheath layer and the region I distance $L_2$ for several different surface voltages can be found in Table 2.

In Fig. 6, we plot the ion current density distributions over platform A which show the leading-edge concentration. This concentration of ion current collection may raise the possibility of serious surface damage such as ion sputtering at the leading edge. If the platform were at a very low voltage, the entire platform would be covered by a fully developed sheath layer. Then the current collection would have a uniform density

$$J_2 \simeq 0.4 e n_0 C_s \simeq 1.3 \times 10^{-2} \text{ mA/m}^2$$

On the other hand, if the platform has a typical surface voltage of $-160$ V, we find that the ion flux density at the leading edge is about 22 times larger than that of a low-voltage surface.

Figure 7 shows the current-voltage characteristic of platform A for a voltage range $10 \text{ V} \leq |\Phi_w| \leq 200$ V. For comparison, we also calculated the *I-V* characteristics for two other platforms with different lengths $L_{\text{tot}}$: platform 2 has a length $L_{\text{tot}} = 4$ m and platform 3 has a length $L_{\text{tot}} = 100$ m. For a long plate, the leading-edge current $I_1$ becomes insignificant at a low voltage because of the very thin sheath. In such a situation, the current collection is dominated by the ion saturation current $I \simeq 0.4 e n_0 C_s \times$ area. Therefore, the *I-V* curve of platform 3 becomes insensitive to the surface voltage at low $|\Phi_w|$. On the other hand, for a short plate at $|\Phi_w| \gg 1$, the current collection is dominated by the leading-edge current $I_1$ because the sheath becomes very thick. For platform 2 the sheath thickness grows to a scale comparable to $L_{\text{tot}}$ at a high voltage.

**Table 2 Sheath thickness, region I distance, leading current, and total current collection at each side of platform A**

| $\Phi_w$, V | $d_{\text{sh}}$, m | $L_2$, m | $I_1$, mA | $I$, mA |
|---|---|---|---|---|
| $-10$ | 0.24 | 1.9 | 0.6 | 3.5 |
| $-50$ | 0.82 | 6.4 | 2.1 | 8.2 |
| $-100$ | 1.37 | 10.8 | 3.4 | 15.8 |
| $-160$ | 1.95 | 15.4 | 4.9 | 22.4 |
| $-200$ | 2.31 | 18.2 | 5.9 | 32.8 |

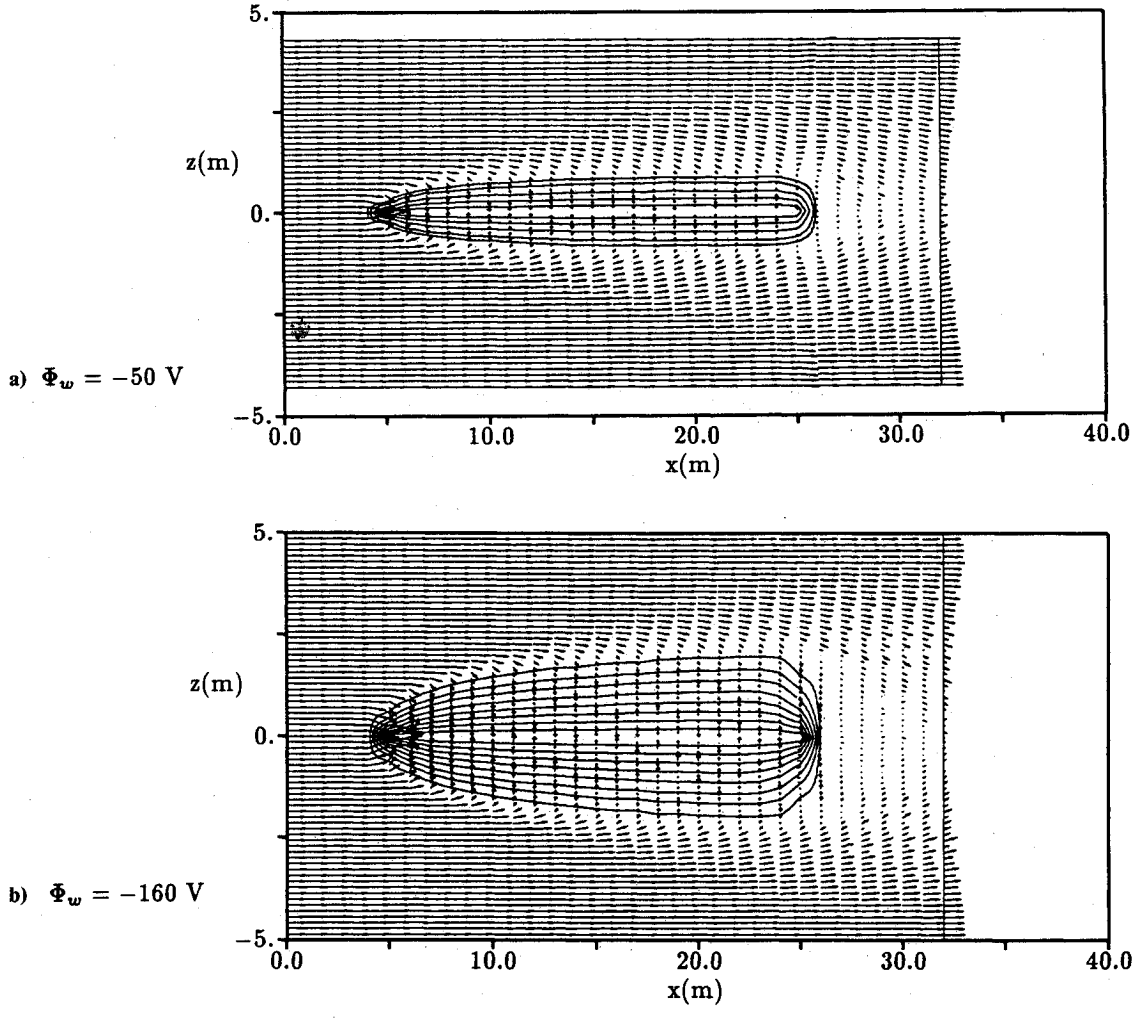


**Fig. 5 Vector map of ion flux *nu* and the sheath around platform A in an $(x_1', x_3')$ plane (contour levels are uniformly distributed between $\Phi = -0.1$ V and $\phi_w$): a) surface voltage $\Phi_w = -50$ V; and b) surface voltage $\Phi_w = -160$ V.**

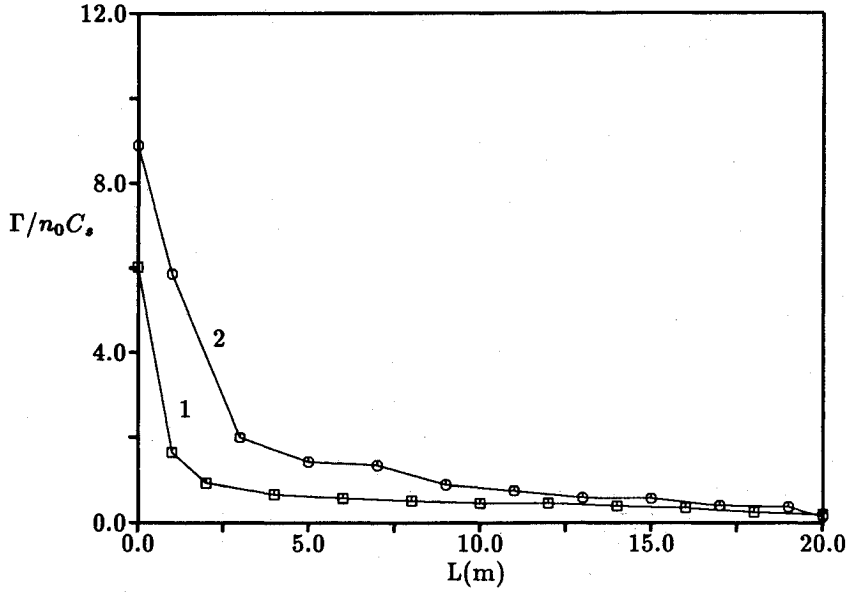


**Fig. 6 Ion flux distribution over platform A. Curve 1: $\Phi_w = -50$ V; and curve 2: $\Phi_w = -160$ V.**

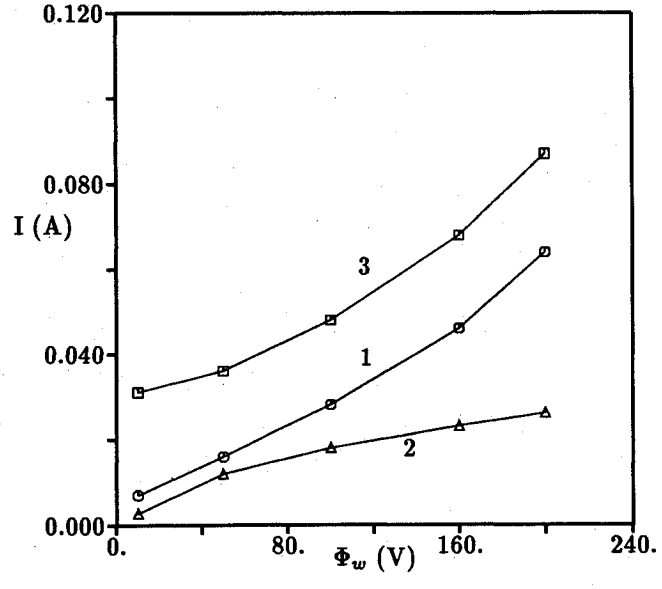


**Fig. 7 Current-voltage characteristics. Current collections are from both side of the platform. Curve 1: platform A; curve 2: platform 2, $L_{tot} = 4$ m; and curve 3: platform 3, $L_{tot} = 100$ m.**

Hence not all the ions entering the sheath will be collected. The ion current collection starts to resemble the characteristics of orbit limited collection.

In our space station model, the electron collection at platform B is simpler than the discussed ion collection at platform A. Since $v_{te} \gg V_0$ and the electrons are strongly magnetized (the Lamor radius $R_{ce} = v_{te}/\Omega_i \simeq 2$ cm), we can apply the theory of a stationary probe in a strong $B$ field (for example, see Refs. 22 and 23). The electron collection in such a situation is mainly from a current tube along the $B_0$ field with the cross section of about the area of the platform. Therefore to a very good approximation, the current exchange at platform B is a uniform current density distributed over the entire surface $J_B = I_{tot}/\text{area}$.

Having analyzed the local interactions at the station's charged platform, we now proceed to a study of the interactions of the entire space station. The governing equation for the far field and the dispersion relation have been discussed in Sec. II. A general calculation of the wave excitation and propagation induced by a space-station-like current source was performed in Ref. 18. It was found that on a time scale $t > \Omega_i^{-1}$, the phenomena observed from the moving frame of the station correspond to an Alfvén wave front $E^A(x')$ propagating across a weak background field of lower hybrid waves along the characteristic lines $z^{\pm}$:

$$E(x',t) \simeq E^A(x')H\left(t - \frac{|z^{\pm}|}{V}\right) \tag{19}$$

$$z^{\pm} = x_1 - V_0 t \pm \frac{V_0}{C_A}|x_3'| = x_1' \pm \frac{V_0}{C_A}|x_3'| \tag{20}$$

where $C_A = B_0/\sqrt{4\pi n_i m_i}$ is the Alfvén speed. The characteristic lines are at an angle of $\theta_A = \tan^{-1}(V_0/C_A)$ with the magnetic field direction. On the time scale $t > \Omega_i^{-1}$, the Alfvén wave appears as a mainly nondispersive wave with $k_3 \simeq \omega/C_A$. The steady-state electric field $E^A(x')$ is established after the wave front has passed, and is given by

$$E_{x'}^A \simeq -\sqrt{2\pi}\frac{C_A}{c^2}\int \boldsymbol{k}\cdot\boldsymbol{j}\frac{k_1}{k_\perp^2}e^{i\psi}\,dk_1\,dk_2$$

$$E_{y'}^A \simeq -\sqrt{2\pi}\frac{C_A}{c^2}\int \boldsymbol{k}\cdot\boldsymbol{j}\frac{k_2}{k_\perp^2}e^{i\psi}\,dk_1\,dk_2$$

$$E_{\parallel}^A \simeq -\sqrt{2\pi}\frac{V_0}{\omega_p^2}\int \boldsymbol{k}\cdot\boldsymbol{j}\,k_1 e^{i\psi}\,dk_1\,dk_2$$

where

$$\psi = \boldsymbol{k}\cdot\boldsymbol{x}' \simeq k_1\left(x_1' \pm \frac{V}{C_A}|x_3'|\right) + k_2 x_2'$$

The $\boldsymbol{j}\cdot\boldsymbol{k}$ terms in the preceding expressions are determined by integrating the current density over the boundary surface of the perturbation source according to

$$\boldsymbol{j}\cdot\boldsymbol{k} = \frac{i}{(2\pi)^{3/2}}\oint \boldsymbol{n}\cdot\boldsymbol{j}e^{-i(\boldsymbol{k}\cdot\boldsymbol{x}')}\,da$$

Note $\boldsymbol{j}\cdot\boldsymbol{k} \neq 0$ only at those surfaces where charge exchange takes place.

One must be careful at choosing the boundary for the current source. Since platform A is usually biased at a very negative voltage, the far-field formulation breaks down within its sheath layer. To be consistent with our far-field formulation, we chose the sheath boundary as the boundary surface of the current source.

Again we consider platform A biased at $-160$ V. The vector map of the current density and the sheath layer were shown in Fig. 5. Rather than a thin platform, the far-field plasma sees platform A as a wedge-shaped current collector. The electric field for such a perturbation source is calculated numerically. Since the electric field is constant along the characteristic lines $z^{\pm} = \text{const}$ once the wave front has passed, we can plot the wave field on any plane perpendicular to $x_3'$ at a distance away from the space station (plane $S_A$ in Fig. 8a). Shown in Fig. 8b is the perpendicular electric field $E_{\perp}^{A}(x') = E_x^A(\hat{x}') + E_{y'}^A \hat{y}' \cdot E_{\perp}^A$ is mainly affected by the perturbation source's structure in the $x_2'$ direction, which is similar to a dipole due to charge exchanges at the two conducting platforms A and B. The detailed structure of the current source in the $x_1'$ direction plays a relatively small role in affecting the overall structure of $E_{\perp}^A$ at far field. This is because the wave number in the $x_1$ direction is determined by the Doppler condition $\omega = k_x V_0$. For the Alfvén wave radiation $\omega < \Omega_i \simeq 31\text{Hz}$, the spatial variation of the Alfvén wave in the $x_1'$ direction is on a scale $\lambda_x > V_0/\Omega_i \sim 2$ km. On the plane $S_A$, the parallel field $E_{\parallel}^A$ is confined within regions $A'$ and $B'$, which are the projections of the current collecting platforms A and B. Outside these regions it approaches zero. The ratio of the average nonzero parallel field to the perpendicular field is $E_{\parallel}^A/E_{\perp}^A \sim 10^{-3}$. This reflects the fact that the plasma is a very good conductor along the magnetic field line. The contours of the magnitude of total field $|\bar{E}^A| = \sqrt{E_{\perp}^{A\,2} + E_{\parallel}^{A\,2}}$ are shown in Fig. 8c. It can be seen that the electric field is concentrated in areas $A$ and $B$. Therefore the radiation field is concentrated within two pairs of "wings" that attach to the two conducting platforms and extend to infinity along the characteristic lines $z^{\pm} = \text{const}$. These are exactly the so-called "Alfvén Wings," which were first described by Drell et al.[24] The induced wave radiation creates an electromagnetic interference in the vicinity of section C (the operation module of our model station). Outside the center point O' of the section C surface (Fig. 8a), the magnitude of the Alfvén wave field per unit current is calculated to be

$$E_{O'}/I_{\text{tot}} \simeq 1.56 \times 10^{-3}\ \text{V} \cdot \text{m}^{-1} \cdot \text{A}^{-1}$$

$E_{O'}$ is the lower bound of the radiation field on the surface of section C. With a total current collection $I_{\text{tot}} \simeq 0.044$ A, we will have an electric interference of $E_{O'} \geq 6.8 \times 10^{-5}$ V/m. Comparing this result with the background field $E_{0'} = V_0 B_0 = 0.24$ V/m, we find the linear assumption is indeed valid in the far field.

Based on our far-field and near-field analyses, we can construct a global picture of the electrodynamic environment of our model space station. The perturbed environment of platform A in a $(x_1', x_3')$ plane is illustrated in Fig. 9. Adjacent to the platform surface there is a sheath layer where the plasma is strongly non-neutral. Outside the sheath there is a presheath of an expansion fan structure, where the environment is dominated by ion sound waves. The sheath and presheath are our near-field zone. The scale of the near-field zone in the $x_3$ direction $R_{\parallel}^{\text{near}}$ can be estimated as the maximum vertical distance from the envelope of the expansion fan to the plate. For $L_{\text{tot}} = 20$ m and $\Phi_w = -160$ V, we have approximately $R_{\parallel}^{\text{near}} \sim d_{\text{sh}} + L_{\text{tot}}/M_0 \simeq 4.5$ m. Far away from the plate we enter the far-field zone, where the dominant phenomenon is the Alfvén wave radiation. The characteristic Alfvén wavelength along $B_0$ is given by

$$\lambda_{\parallel}^{\text{Alfvén}} = \frac{1}{k_3} = \frac{C_A}{k \cdot V_0} \sim \frac{C_A}{V_0} L_{\text{tot}} \simeq 41 L_{\text{tot}}$$

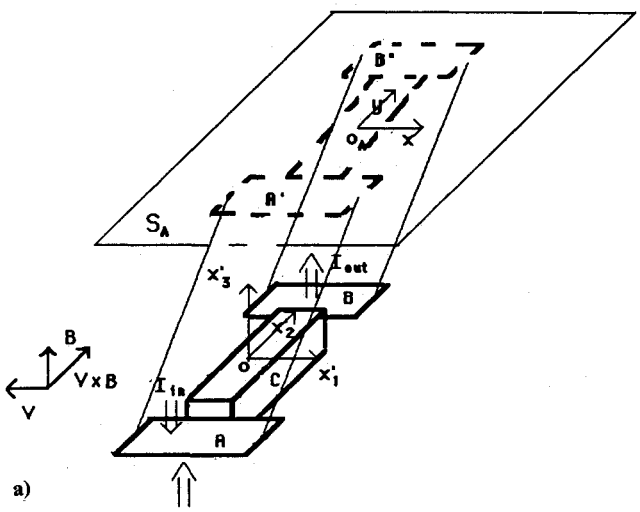


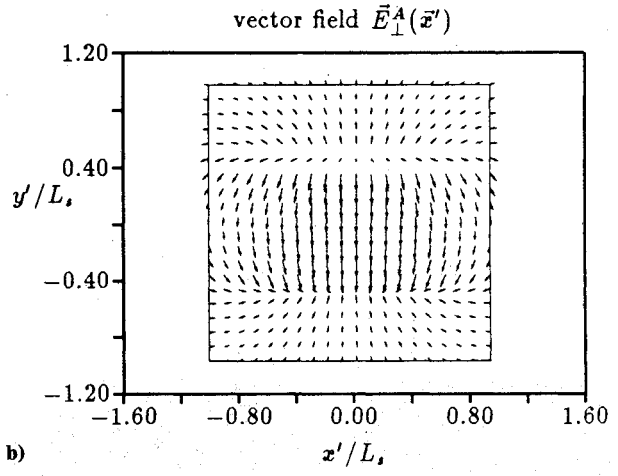


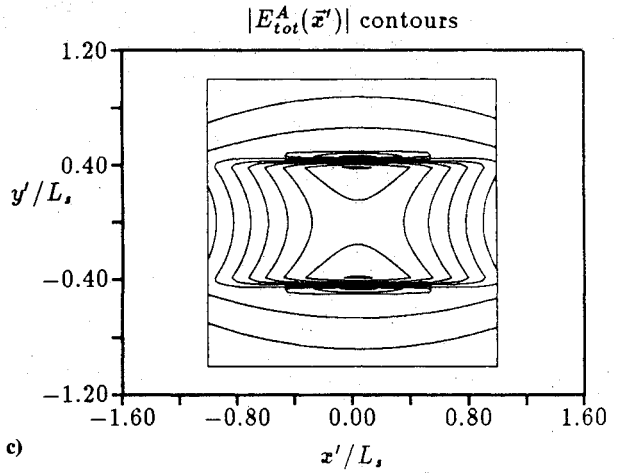


**Fig. 8 Far-field Alfvén wave radiation: a) radiation system; b) and c) vector and contour map of electric field on $S_A$ plane.**

which gives $\lambda_{\parallel}^{\text{Alfvén}} \sim 800$ m for $L_{\text{tot}} = 20$ m. Since the near-field region is well within one Alfvén wavelength ($R_{\parallel}^{\text{near}} \ll \lambda_{\parallel}^{\text{Alfvén}}$), from the discussion in Sec. II we find that the electrostatic approximation in the near field is justified.

It is interesting to compare the potential drop in different zones. Let us draw a vertical line along the $B_0$ direction from the center of platform A (line OP in Fig. 9), which intersects the sheath boundary, presheath envelope, and the frontside Alfvén characteristic line at points M, N, and P. Let us take the surface potential of the platform to be $\Phi_w = -160$ V with

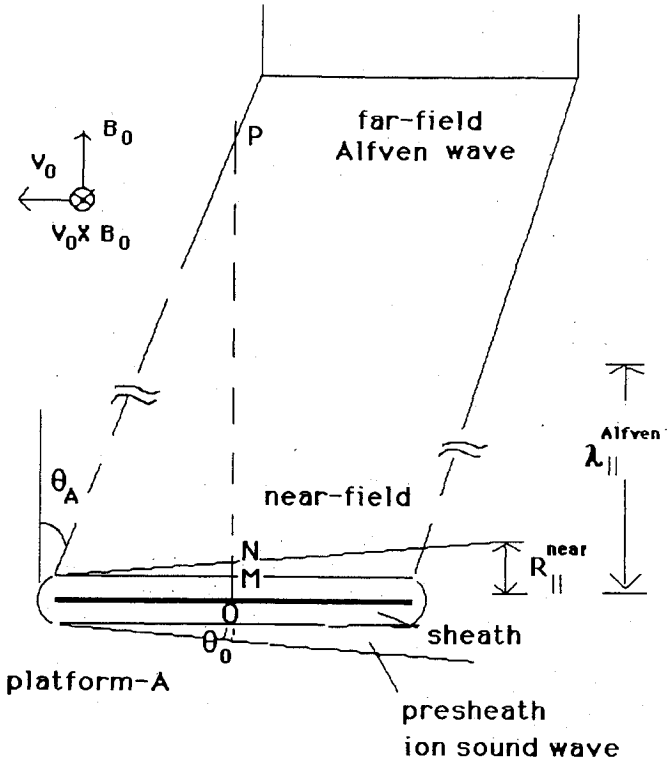


**Fig. 9 Electrodynamic environment of platform A.**

respect to the unperturbed ambient plasma. Since the high voltage of the platform will be mainly shielded within this sheath layer, the sheath potential drop $\Delta\Phi_{sh} = \Delta\phi_{OM} \sim |\Phi_w| \simeq 160$ V. The analysis in Sec. III shows that the potential drop across the expansion fan is of the order of the electron temperature, therefore we have $\Delta\Phi_{presh} = \Delta\Phi_{MN} \sim \mathcal{O}(KT_e/e) \sim 0.1$ V. With a total current collection $I_{tot} \sim 40$ mA by platform A, we find the average parallel field in the far-field zone to be $E_{\|}^{A} \sim 10^{-7}$ V/m. Integration of $E_{\|}^{A}$ along line PN, we obtain $\Delta\Phi_{PN} \sim 10^{-5}$ V. Hence, we have $\Delta\Phi_{far} \ll \Delta\Phi_{presh} \ll \Delta\Phi_{sh}$.

One of the key assumptions in our approach is that the effects of far-field interactions are negligible in determining the near-field solution, and therefore, the far-field and near-field problem can be decoupled. From the previous discussion, it is obvious that the interactions in different zones are at different levels. We can also compare the radiation power carried by the far-field waves $P_{rad}$ with that dissipated in the near field of platform A $P^{near}$. The far-field power radiation can be calculated by integrating the Poynting vector over a surface enclosing the entire space station:

$$P_{rad} = \int (\boldsymbol{E} \times \boldsymbol{B}) \cdot d\boldsymbol{S} = I_{tot}^2 \, Z_{rad} \tag{21}$$

where $Z_{rad} = Z_I + Z_{II}$ is the radiation impedance. This calculation is performed using an algorithm elaborated in Ref 9. For our space station model, we found the radiation impedance associated with the Alfvén wave: $Z_I \simeq 0.055\ \Omega$ and the impedance for the lower hybrid waves $Z_{II} \simeq 0.0028\ \Omega$. The near-field power drain of platform A is the sum of that in the sheath and presheath $P_{near} = P_{presh} + P_{sh}$, where

$$P_{sh} \simeq I_{tot} \, \Delta\Phi_{sh} \simeq I_{tot} |\Phi_w| \tag{22}$$

$$P_{presh} \simeq I_{tot} \, \Delta\Phi_{presh} \simeq I_{tot} \frac{KT_e}{e} \tag{23}$$

For $|\Phi_\omega| = 160$ V and $I_{tot} = 44$ mA, we find $P_{rad} \simeq 10^{-4}$ W, $P_{presh} \simeq 4.4 \times 10^{-3}$ W, and $P_{sh} \simeq 7$ W. Hence, we have

$$P_{rad} < P_{presh} \ll P_{sh}$$

Therefore, the condition for decoupling the far field and the near field, Eq. (8), is satisfied.

## V. Discussions and Conclusions

In this paper, we have adopted a separate approach to the problem; i.e., we first solve the interactions in the vicinity of the charged plates (governed by the Poisson's equation and the plasma kinetic equations); we then construct a perturbation current source and solve the far-field interactions (governed by Maxwell's equations and the linearized cold plasma fluid equations). A separate treatment of the different interaction regions greatly simplifies our analysis. As summarized in Table 3, we find our approach and assumptions are well justified by the results.

In this paper, our solution of presheath is not yet connected to that of the far-field zone. The transition from the far-field solution to the presheath solution can be seen clearly from the relative importance of the effects of the magnetic field and the plasma temperature. For example, let us perform a scale analysis for the environment of the negatively charged platform A (Fig. 9). To a good approximation we may simply use the magnetohydrodynamic (MHD) equations for such an analysis in the far-field zone. We find the dominant driving force term in the far-field zone is the $\boldsymbol{j} \times \boldsymbol{B}$ term. The ratio of this term to the plasma pressure term is found to be

$$\left|\frac{\boldsymbol{j} \times \boldsymbol{B}}{KT \nabla n}\right|_{far} \sim \frac{jB_0 L_{far}}{KT\delta n} \sim \left(\frac{V_0}{C_s}\right)^2 \gg 1$$

However, as we move closer and closer to the charged plate, this ratio gradually changes to less than one. In the presheath region, taking the length scale to $L_{presh} \sim L_{tot}/M_0$ and the current $j \sim eC_s n_0$, we found

$$\left|\frac{\boldsymbol{j} \times \boldsymbol{B}}{KT \nabla n}\right|_{presh} \sim \frac{eC_s B_0 L_{presh}}{KT} \sim \left(\frac{L_{tot}}{R_{ci}}\right)^s < 1$$

where $R_{ci} = V_0/\Omega_i$. Therefore the transition of the space station's electrodynamic environment from the far-field zone to the presheath is such that the dominant characteristics of the environment change from those of a mainly cold, magnetized plasma to a mainly warm, unmagnetized plasma. The transition from our far-field solution to the presheath is through an intermediate zone, where both the effects of the magnetic field and the plasma temperature are important. In principle, the interactions in the intermediate zone may be solved numerically by extending the hybrid-particle method in the following way: 1) enlarging the particle simulation domain; 2) simulating a magnetized, warm plasma; and 3) imposing a radiation boundary condition to feed into the effects of far-field waves. This task is still a subject of ongoing research.

We want to emphasize that the validity of our approach and solution strictly depends on the dimensions of the system and the magnitude of the total current collection. For instance, we now consider the current collection of our space station when controlled by means of active electron beam emission. We still take the surface voltage of platfrom A to be $\Phi_w = -160$ V. In

**Table 3 Comparison of the assumptions and results**

| Assumptions | Results |
|---|---|
| Eq. (3): $E_{rad}/V_0 B_0 \|_{far} \ll 1$ | $E_{rad} \sim 10^{-5}$ V/m, $V_0/B_0 \simeq 0.24$ V/m |
| Eq. (6): $R^{near} \ll \lambda_{wave}$ | $R_{\|}^{near} \sim 4$ m, $\lambda_{\|}^{Alfvén} \sim 800$ m |
| Eq. (8): $P_{rad} \ll P_{near}$ | $P_{rad} \simeq 10^{-4}$ W, $P_{near} \simeq 7$ W |

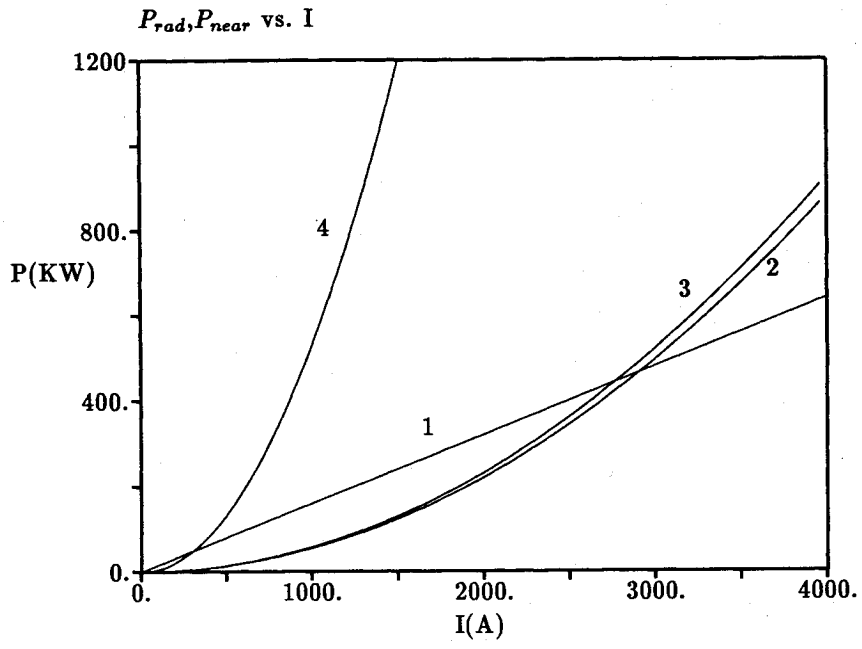


**Fig. 10 Comparison of $P_{rad}(I)$ and $P_{near}(I)$: curve 1 $P_{near} = I\Delta\Phi$ ($\Delta\Phi$ = 160 V); curve 2 $P_{Alfvén} = I^2Z_I$; curve 3 $P_{rad} = I^2(Z_{II} + Z_{II})$ ($L_{tot}$ = 20 m); and curve 4 $P_{rad} = I^2(Z_I + Z_{II})(L_{tot} = 2$ m).**

Fig. 10 we plot the total power radiation $P_{rad} = I^2(Z_I + Z_{II})$, the Alfvén wave power radiation $P_{Alfvén} = I^2Z_I$, and the near-field power $P_{near} = I|\Phi_w|$ as functions of the current collection. Our near-field formulation requires $P_{rad} \ll P_{near}$ in the environment of platform A, which sets an upper bound on current collection $I < |\Phi_w|/Z_{rad} \sim I_c^{near}$. Our far-field formulation sets a second upper bound on the current collection because the strength of the radiation field is proportional to the current magnitude. The linear assumption requires the current collection to be much less than $I_c^{far}$, which is obtained from $E(I_c^{far}) \sim V_0B_0 \simeq 0.24$ V/m. Hence, for an active system, our approach is valid only when the current magnitude satisifes

$$I \ll \min(I_c^{near}, I_c^{far}) = I_c$$

For our space station model, we find $I_c^{near} \sim 3.5 \times 10^2$ A and $I_c^{far} \sim 10^2$ A, which gives $I_c \sim 10^2$ A. Therefore the picture of the electrodynamic environment constructed in the last section breaks down if our space station model actively emits a current $I > I_c \sim 10^2$ A. Physically, this is to be expected because strong electron beam emission will generate nonlinear perturbations throughout both the near-field and far-field zones. We would like to point out that $I_c$ also depends on the dimension of the electric contact of the space station. For instance, we now consider a similar structure but with $L_{tot} = 2$ m instead of 20 m. We have calculated the radiation impedance for this structure. The radiation impedance for the Alfvén band is still $Z_I \simeq 0.055\ \Omega$; however, the radiation impedance in the lower hybrid band is much higher due to the shorter $L_{tot}$: $Z_{II} \simeq 0.47\ \Omega$. Hence the far field is dominated by the radiation in the lower hybrid band instead of the Alfvén band. The total power radiation $P_{rad}$ as a function of the current is also plotted in Fig. 10. We find the current bound $I_c$ for a structure with smaller charged parts is much less than that with larger ones.

In conclusion, we have presented a general analysis of the electrodynamic interactions between a space station and the ionospheric plasma environment. Our study includes both the interactions at the vicinity of the charged parts and the interactions at a scale surrounding the space station. Results are obtained for the plasma flowfield, the presheath/sheath structure around the space station's charged platform, and the Alfvén wings attached to the entire station. The current collection, near-field power drain, and overall electromagnetic interference are also discussed. Based on our analysis, we have obtained a global picture of the space station's electrodynamic environment. In this paper we only considered a very simplified model space station. More sophisticated space station models, including detailed microscale interactions, space station grounding, as well as transient phenomena, are still needed.

## Acknowledgments

This work was supported by NASA Grant NAG 3-695. The authors would like to thank E. Ahedo and H. B. Garrett for many useful discussions and suggestions.

## References

[1]Garrett, H. B., "The Charging of Spacecraft Surfaces," *Review of Geophysics,* Vol. 19, No. A2, 1981, pp. 577–616.

[2]Neubert, T., Mandell, M. J., Sasaki, S., Gilchrest, B. E., Banks, P. M., Williamson, P.R., Riatt, W. J., Meyers, N. B., Oyama, K. I., and Katz, I., "The Sheath Structure Around a Negatively Charged Rocket Payload," *Journal of Geophysical Research,* Vol. 95, No. A2, 1990, pp. 6155–6166.

[3]Katz, I., Mandell, M. J., Parks, D. E., Wright, K., Stone, N. H., and Samir, U., "Effect of Object Potentials on the Wake of a Flowing Plasma," *Journal of Applied Physics,* Vol. 62, No. 7, 1987, pp. 2675–2679.

[4]Senbetu, L., and Henley, J., "Distribution of Plasma Density and Potential Around a Mesothermal Ionsopheric Object," *Journal of Geophysical Research,* Vol. 94, No. A5, 1989, pp. 5441–5448.

[5]Stone, N. H., "The Aerodynamics of Bodies in a Rarefied Ionized Gas with Applications to Spacecraft Environmental Dynamics," NASA TP 1933, 1981.

[6]Barnett, A., and Olbert, S., "Radiation of Plasma Waves by a Conducting Body Moving Through a Magnetized Plasma," *Journal of Geophysical Research,* Vol. 91, No. A9, 1986, pp. 10117–10135.

[7]Rasmussen, C. E., Banks, P. M., and Harker, K. J., "The Excitation of Plasma Waves by a Current Source Moving in a Magnetized Plasma: The MHD Approximation," *Journal of Geophysical Research,* Vol. 90, No. A1, 1985, pp. 505–515.

[8]Estes, R. D., "Alfvén Waves from an Electrodynamic Tethered Satellite System," *Journal of Geophysical Research*, Vol. 93, No. A2, 1988, pp. 945–956.

[9]Hastings, D. E., and Wang, J., "Induced Emission of Radiation from a Large Space Station-Like Structure in the Ionosphere," *AIAA Journal,* Vol. 27, No. 4, 1989, pp. 438–445.

[10]Kuninaka, H., and Kuriki, K., "Interference of High Voltage Solar Array with Ionospheric Plasma," *Proceedings of the 15th Inter-*

*national Symposium on Space Technology and Science,* Tokyo, Japan, May 1986, pp. 819–824.

[11]Hastings, D. E., and Cho, M., "Ion Drag for a Negatively Biased Solar Array in Low Earth Orbit," *Journal of Spacecraft and Rockets,* Vol. 27, No. 3, 1990, pp. 279–284.

[12]Thiemann, H., and Schunk, R. W., "Particle-In-Cell Simulation of Sheath Formation Around Biased Interconnectors in a Low-Earth-Orbit Plasma," *Journal of Spacecraft and Rockets,* Vol. 27, No. 3, 1990, pp. 554–562.

[13]Katz, I., Jongeward, G. A., Davis, V. A., Mandell, M. J., Kuharski, R. A., Lilley, J. R., Raitt, W. J., Cooke, D. L., Torbert, R. B., Larson, G., and Rau, D., "Structure of the Bipolar Plasma Sheath Generated by Spear 1," *Journal of Geophysical Research,* Vol. 94, No. A2, 1989, pp. 1450–1458.

[14]Katz, I., Mandell, M. J., Parks, D. E., and Steen, P.G., "Plasma Collection by High-Voltage Spacecraft at Low Earth Orbit," *Journal of Spacecraft and Rockets,* Vol. 18, No. 1, 1981, pp. 79–82.

[15]Mandell, M. J., Katz, I., Jongeward, G. A., and Roache, J. C., "Computer Simulation of Plasma Electron Collection by PIX-II," *Journal of Spacecraft and Rockets,* Vol. 23, No. 5, 1986, pp. 512–518.

[16]Davis, V. A., Katz, I., Mandell, M. J., and Parks, D. E., "Hollow Cathodes as Electron Emitting Plasma Contactors: Theory and Computer Modeling," *Journal of Spacecraft and Rockets,* Vol. 25, No. 2, 1988, pp. 175–179.

[17]Davis, V. A., Mandell, M. J., and Katz, I., "Electron Collection by Multiple Objects Within a Single Sheath," *Journal of Spacecraft and Rockets,* Vol. 25, No. 1, 1988, pp. 94–95.

[18]Wang, J., and Hastings, D. E., "A Dynamic Analysis of the Radiation Excitation from the Activation of a Current Collecting System in Space," *Journal of Geophysical Research,* Vol. 96, No. A3, 1991, pp. 3611–3620.

[19]Lam, S., and Greenblatt, M., "On the Interaction of a Solid Body with a Flowing Collisionless Plasma," *The Fourth Symposium Rarefied Gas Dynamics II,* Academic, New York, 1966, pp. 45–61.

[20]Wang, J., "Electrodynamic Interactions Between Charged Space Systems and the Ionospheric Plasma Environment," Ph.D. Thesis, Massachusetts Inst. of Technology, Cambridge, MA, June 1991.

[21]Wang, J., and Hastings, D. E., "Ionsopheric Plasma Flow Over Large High-Voltage Space Platforms. 2. The Formation and Structure of the Plasma Wake," *Physics of Fluids,* Vol. 4, No. 6, 1992, pp. 1615–1629.

[22]Bertotti, B., "Theory of an Electrostatic Probe in a Strong Magnetic Field," *Physics of Fluids,* Vol. 4, No. 8, 1961, pp. 1047–1052.

[23]Parker, L. W., and Murphy, B. L., "Potential Buildup on an Electron Emitting Ionspheric Satellite," *Journal of Geophysical Research,* Vol. 72, No. 5, 1967, pp. 1631–1636.

[24]Drell, S. D., Foley, H. M., and Ruderman, M. A., "Drag and Propulsion in the Ionosphere: an Alfvén Engine in Space," *Journal of Geophysical Research,* Vol. 70, No. 13, 1965, pp. 3131–3145.

Antoni K. Jakubowski
*Associate Editor*